J. Synchrotron Rad. (2000). **7**, 221–228

A novel application of silicon microstrip technology for energy-dispersive EXAFS studies

G. Iles,[a]* A. Dent,[b] G. Derbyshire,[c] R. Farrow,[b] G. Hall,[a] G. Noyes,[c]† M. Raymond,[a] G. Salvini,[b] P. Seller,[c] M. Smith[c]† and S. Thomas[c]

[a]Blackett Laboratory, Imperial College, London SW7 2BZ, UK, [b]CLRC, Daresbury Laboratory, Daresbury, Warrington WA4 4AD, UK, and [c]CLRC, Rutherford Appleton Laboratory, Chilton, Didcot, Oxon OX11 0QX, UK. E-mail: gm.iles@ic.ac.uk

(*Received 14 November 1999; accepted 5 April 2000*)

A prototype X-ray detector for energy-dispersive EXAFS has been developed and tested to demonstrate the principle of using silicon microstrip detector technology for this application. Testing took place at the UK Synchrotron Radiation Source, where the absorption spectra of a 5 μm Ni foil and a 25 m*M* $NiCl_2$ solution were obtained.

Keywords: energy-dispersive EXAFS; EDE; silicon; microstrips; X-rays.

1. Introduction

Extended X-ray absorption fine structure (EXAFS) is a component of the absorption spectrum in the X-ray region that can be used to determine the local atomic structure of a material. It occurs as absorption modulation on the high-energy side of a photoelectric absorption edge. Details such as bond distance, structural disorder, coordination number and the chemical identity of the coordinating atom can all be obtained using this method (Lytle *et al.*, 1982). EDE (energy-dispersive EXAFS) is a technique that allows the absorption spectrum to be measured quickly and simultaneously. A spatially dispersed polychromatic X-ray beam, hereafter referred to as an X-rainbow, is generated by an X-ray beam incident on a bent Si crystal monochromator (Fig. 1). X-rays diffracted from the crystal are restricted by the Bragg condition so that as the angle of incidence increases across the incident fan of radiation so does the wavelength. The resulting X-rainbow is typically 0.5–1 keV wide and converges to a point 75–120 cm away, where the sample is placed. As the X-rainbow emerges from the sample, the absorption spectrum is superimposed upon it. A linearly segmented detector placed a further 1 m away records the X-rainbow and hence the absorption spectrum. The detector parameters are set by the X-ray source and the optics used to form the X-rainbow. The latter has a width of 2–3 cm in the dispersion dimension and a height of a few hundred micrometres at the sample.

The detector system must measure the X-ray intensity to a high precision because the EXAFS component of the absorption spectrum can be very small. A signal-to-noise ratio (SNR) of at least 10^3 is normally required, and a value greater than 10^6 is quoted as necessary for the highest-quality data (Allinson, 1989). Further improvements in detector performance would allow materials with weaker EXAFS signals to be studied. Time-resolved experiments allow the structure of a material to be studied as a chemical change takes place. The rate at which these reactions occur can vary from minutes down to a few tens of nanoseconds. The current minimum time period for good quality data is a few tens of milliseconds from the photodiode arrays used at the UK Synchrotron Radiation Source (SRS) (Dobson, 1997). This minimum time scale is ultimately set by the rate at which photons can be detected, which is a function of both X-ray beam and detector performance.

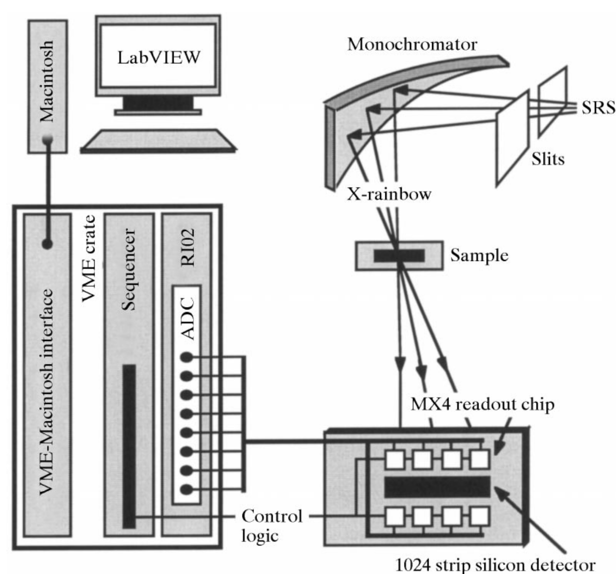

Figure 1
Experimental set-up for energy-dispersive EXAFS experiments, the silicon microstrip detector and data acquisition system.

† No longer at CLRC, Rutherford Appleton Laboratory.

© 2000 International Union of Crystallography
Printed in Great Britain – all rights reserved

The inherent Poisson statistical error in counting N photons is simply $N^{1/2}$. This is normally the dominant error and places a fundamental limit on the minimum number of photons that have to be measured and hence the time interval required. Consequently, for an SNR of 10^6 and high-quality data, 10^{12} photons need to be integrated per detecting element. It is therefore often necessary to accumulate many measurements, known as scans, into frames to build up sufficient photon statistics. To achieve this the statistical and systematic noise from the detector and electronics needs to be significantly less than the inherent Poisson error. The statistical noise will add in quadrature when many scans are combined to form a frame and hence the statistical noise per scan has the same requirement as it does per frame (*i.e.* it has to be less than the Poisson error). The systematic noise sources pose a much greater challenge if they cannot be determined and corrected for because the error in each scan will combine linearly when many scans are combined into a frame. It is these systematic errors which inevitably limit an integrating system. The energy resolution of energy-dispersive experiments is determined by both the beam optics and the detector spatial resolution.

At the SRS these detector requirements are presently achieved with commercially available photodiode arrays (PDAs) manufactured by EG & G Reticon Opto-electronics, USA, and Hamamatsu Photonics KK, Japan. Over the past decade these have been incorporated into a high-quality fully supported system that is well matched to the current flux of up to 10^{11} photons s^{-1} across the entire detector (Allinson, 1989; Allinson *et al.*, 1988; Bogg *et al.*, 1997). These detectors are similar to the microstrip detectors because they both use a series of reverse-biased diodes as the detecting elements, although there are significant differences. The PDAs operate at low reverse bias and are fabricated on low-resistivity silicon compared with the 5 kΩ cm typical of microstrip detectors. Consequently, the depth of the depletion region is less than 1 μm and thus charge collection must occur by either slow drift in the weak electric field that extends beyond the depletion region or by diffusion. A large fraction of the charge generated in the undepleted region may therefore be lost. For X-ray energies of a few keV, absorption occurs close to the photodiode surface and a large fraction of the charge will be collected whereas for higher-energy X-rays absorption occurs throughout the detector and therefore a smaller fraction of the charge will be collected. The charge collected per photon may therefore be non-uniform as a function of absorption depth within the detector. The lateral, as well as vertical, diffusion of charge can also lead to a reduction in detector spatial resolution, although this effect is lessened because charge generated a large distance from the photodiode junction is unlikely to diffuse or drift to the photodiode depletion volume.

At station ID24 on the ESRF (Koch *et al.*, 1995; Hagelstein *et al.*, 1997; Dent, 2000), X-rays are detected by a 40 μm-thick P43 (Gd_2O_2S:Th) or 80 μm-thick P46 ($Y_3Al_5O_{12}$:Ce) powdered phosphor which is placed at 45° to the incident X-rays. A couple of lenses focus the light emitted onto several lines of a 1242 × 1152 pixel CCD. The remaining unexposed parts of the CCD are used to store successive spectra by shifting through the 1152 lines of the CCD. In practice, 64 lines of the CCD are required per spectrum to record the data and to reduce cross-talk between the scans to within acceptable limits. Consequently, 18 spectra can be recorded for a readout period of 400 ms.

The two potential drawbacks of using phosphors are the loss in spatial resolution and the time taken for the light to decay, which is often comprised of more than one component. Measurements made with P43 by alternate 5 ms periods of exposure/shielding showed that the time taken for the light to decay to half of its amplitude was 400 μs, which fell to less than 100 μs with P46. The relative amplitude of the signal after 10 min exposure followed by 1 min shielding was 10^{-6} for P43 and 10^{-3} for P46. The spatial resolution was measured by illuminating the detector with a collimated 20 μm-wide line image. The size of the detector was 40 mm wide and 0.8 mm high, but only half was imaged onto the CCD, presumably because the lens system was designed for a future upgrade to a larger CCD. The larger CCD would double the energy range and the number of spectra that could be recorded. FWHM values of 60 μm and 80 μm were recorded for the P43 and P46 phosphors, respectively, though the spatial distribution was non-Gaussian. The signal fell to 10^{-3} of its maximum value after a distance of ∼0.2 mm (P43) and ∼0.3 mm (P46) from the line image. This is equivalent to 1% (P43) or 1.5% (P46) of the full detector width. Spatial resolution can be improved by reducing the phosphor thickness, but this is also accompanied by a reduction in detection efficiency and consequently a compromise is necessary.

Silicon microstrips are a possible alternative, pioneered for particle physics. They potentially offer short measurement times due to a thick active volume, and hence a large absorption cross section. For a 600 μm-thick detector they offer 99% photon detection efficiency up to 10 keV and

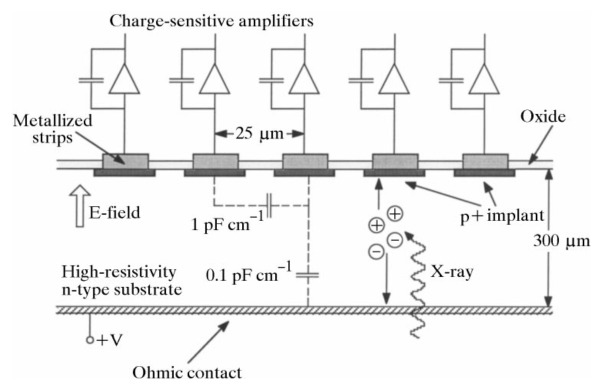

Figure 2
Cross section through a typical silicon detector diode showing the radiation-sensitive field oxide and the X-rays, on this occasion incident on the back.

more than 43% efficiency up to 20 keV. They can also operate in, and hence take advantage of, the high X-ray flux produced by third-generation synchrotron sources such as DIAMOND, the new UK synchrotron source to replace the SRS. The PDA detectors would saturate at a third-generation source because their minimum integration period is too long. The latter is set by the chip architecture, in which each detecting element is sequentially read out and reset. The minimum period for readout/integration is therefore set by the time taken to pass through all detecting elements which is currently 0.5 ms on the present PDA system (Bogg *et al.*, 1997).

For silicon detectors the spatial resolution is set by the strip pitch, the size of the detector (*i.e.* number of strips $\times$ pitch) and the lateral diffusion of charge, created by X-ray absorption, as it drifts in the E-field of the reverse-biased diode (Fig. 2). For X-rays absorbed on the opposite side of the detector to the readout strips the charge must drift through the full detector thickness. By applying a reverse bias that is much greater than the voltage necessary to fully deplete the detector, it is possible to speed up the drift velocity and hence limit the time for diffusion. As the size of the initial ionization cloud is only a few micrometres for X-ray energies of $\sim$10 keV (Fitting, 1974), it can be considered initially as a point source, and the size of the diffusion cloud on reaching the readout strips is given by

$$\sigma = (2D_p t)^{1/2}, \qquad (1)$$

where D_p is the carrier diffusion coefficient for holes (or D_n for electrons) and t is the time taken to drift across the readout strips.

Assuming that we have a high-resistivity 300 μm-thick detector with a depletion voltage that is small compared with the over-bias voltage of 300 V, then the E-field strength is 10^4 V cm^{-1} throughout the detector and the hole drift velocity is 3×10^6 cm s^{-1} (Sze, 1981). Given that the hole diffusion coefficient for this material is 11.7 cm^2 s^{-1} (Sze, 1981), then the RMS spread of the charge cloud on reaching the readout strips is 4.8 μm and the FWHM is 11.5 μm. This is comparable with a strip pitch of 25 μm, and hence a smaller pitch, even if it were possible, would not yield a much better energy resolution.

For a precise calculation of the size of the diffusion cloud there are a number of other factors that should be included, such as integrating over all interaction depths and the probability of an interaction at that depth. The latter depends on the incident X-ray energy and whether the readout-strip side or back faces the incident radiation. These factors can reduce the size of the charge cloud, as can increasing the reverse-bias voltage, although this is typically limited to $\sim$500 V at present.

Conversely, the size of the charge cloud will increase if the detector thickness is increased because the charge has to drift through a further distance allowing a longer time for charge diffusion. Furthermore, a larger portion of the reverse-bias voltage will be necessary to fully deplete the detector, allowing only a small over-bias voltage, and thus

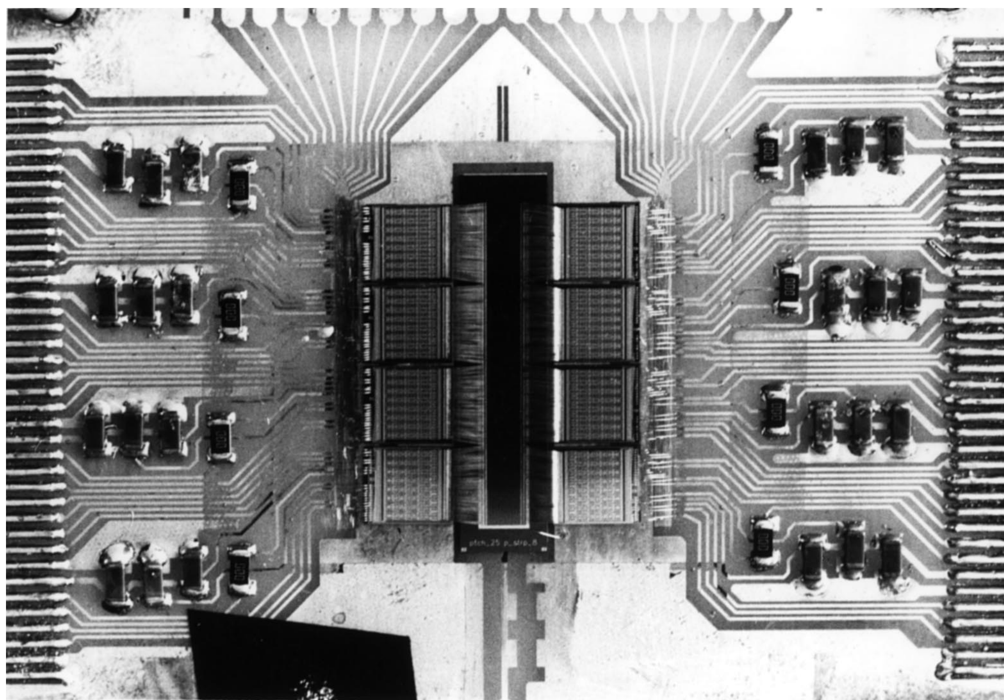

Figure 3
The silicon detector is shown mounted in the centre of the hybrid with the MX4 chips on either side. A sense of scale can be obtained from the detector which has dimensions 7 mm $\times$ 30 mm, although it should be noted that the active area is less than this.

the simple approximation made above of a constant E-field throughout the detector is no longer valid. For very thick detectors (*e.g.* 1 mm-thick), charge diffusion may therefore become more important than strip pitch.

For E-fields below 3×10^3 V cm^{-1} the size of the charge cloud reaching the readout strips will be the same for both electrons and holes because, although the diffusion coefficient is higher for electrons owing to their higher mobility, this is cancelled by the shorter time taken to reach the readout strips, again owing to their higher mobility. Above 3×10^3 V cm^{-1} the drift velocity of electrons starts to saturate and, although the drift velocity of holes also starts to saturate, it takes place more slowly. For an E-field of 10^5 V cm^{-1}, the drift velocity of holes starts to approach that of electrons. Consequently, the time taken to reach the readout strips is the same for both electrons and holes, but the hole diffusion coefficient is approximately one-third of that of the electron and thus the charge cloud is smaller. Hole collection is therefore preferred over electron collection and it should be noted that the benefits of a higher bias voltage will become less as the drift velocities of electrons and holes saturate.

The remaining factor that determines the energy resolution is the size of the detector (*i.e.* number of strips × pitch). At present the largest high-resistivity wafers being fabricated have a diameter of ~15 cm. Consequently, the maximum number of strips assuming a 25 µm pitch is ~5000. A single strip therefore represents 0.02% of the full detector length and, because charge diffusion is confined to approximately a strip width, the spatial resolution should be excellent. If the benefits of a silicon microstrip-based detector are to be fully exploited, they will require a readout chip with front-end electronics well matched to the application and which operates with negligible dead time.

The purpose of this work was to test the principle of a silicon microstrip-based detector for EDE with a collaboration between CLRC and Imperial College.

2. Silicon microstrip detector and readout system

This system comprised a 1024-strip detector, designed at Imperial College and then manufactured by the Atomic Energy Authority, UK, from masks produced by the Central Microstructure Facility at Rutherford Appleton Laboratory. The detector was single sided, DC coupled and had 1024 strips, each 2.5 mm long on a pitch of 25 µm. The silicon substrates were supplied by Wacker Chemitronic, Germany, and Topsil Semiconductor Materials, Denmark, with orientation and thickness ⟨111⟩, 350 µm and ⟨100⟩, 300 µm, respectively.

Eight MX4 chips, originally developed for the Delphi micro-vertex detector at CERN, read out the 1024-strip detector (Fig. 3). To match the 25 µm strip pitch on the detector to the 50 µm amplifier input pitch on the MX4 chips, the latter were placed either side of the detector and thus each MX4 read out only odd or even strips. Each of the 128 input channels of the MX4 contained a charge-sensitive amplifier that integrated charge generated by X-rays incident on a detector strip. The voltage output from each amplifier was sampled before and after the integration period on two capacitors. The voltage difference between these two capacitors, which represented the charge created in each strip and thus the number of incident photons, was then multiplexed out onto an analogue bus at 2 MHz. The technique, known as double correlated sampling, had the advantage that common mode signals were removed, as was low-frequency noise. The 1.4 pF feedback capacitor on each charge-sensitive amplifier allowed a charge of 1.4×10^7 electrons to be integrated per strip, which is equivalent to 5040 10 keV photons.

A VME sequencer module provided the control logic for the MX4 readout chips. The analogue data stream from

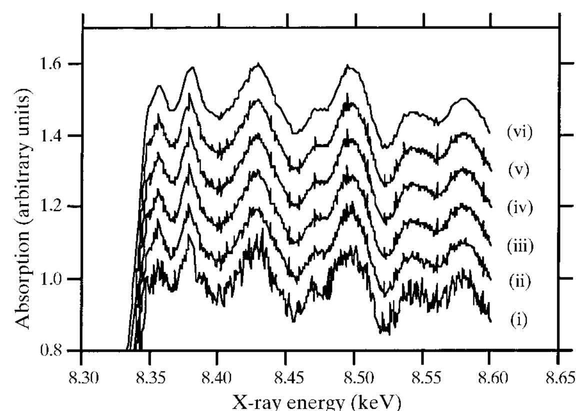

Figure 4
The absorption spectra obtained from the Ni foil with (i) 1 scan, (ii) 10 scans, (iii) 100 scans, (iv) 1000 scans, (v) 10000 scans and (vi) 10000 scans with odd and even channels averaged. The data sets are offset vertically by 0.1 units for clarity. Acquisition times per scan are I_t = 250 µs and I_0 = 100 µs.

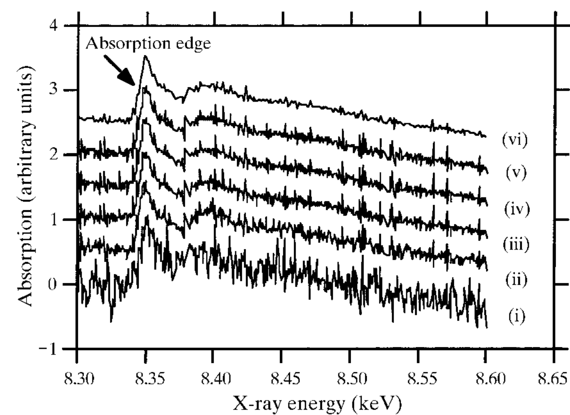

Figure 5
The absorption spectra obtained from the $NiCl_2$ solution with (i) 1 scan, (ii) 10 scans, (iii) 100 scans, (iv) 1000 scans, (v) 10000 scans and (vi) 10000 scans with odd and even channels averaged. The data sets are offset vertically by 0.5 units for clarity. Acquisition times per scan are I_t = 1 ms and I_0 = 150 µs.

each MX4 chip was buffered before being digitized by an ADC (RIO2 FADC PMC), originally developed at Rutherford Appleton Laboratory, UK, for silicon tracking detectors in the H1 particle-physics experiment at HERA, Germany. The module had eight 12-bit ADC channels which allowed the multiplexed analogue output of each MX4 chip to be digitized and stored in dual port memory. All the channels were digitized within 64 μs. A programmable FPGA chip summed the data from multiple scans (integration periods) into a frame. Data were forwarded to a Creative Electronic Systems RIO2 8060 VME module where a Power PC processor reordered them. The computer running National Instruments LabVIEW software retrieved the data and provided a simple interface for the user to control the system.

3. Results

The system was tested on the Material Science Station 9.3 at the SRS (Derbyshire *et al.*, 1989). The station provided an intense X-ray source in the region 6–30 keV. To create the X-rainbow necessary for EDE experiments, a bent triangular Si(111) crystal monochromator was used. The sample and detector both sat on a 2θ instrumentation arm which swung out to intercept the beam. In this way an energy range of 8.3–8.7 keV was selected.

Results were first obtained with an Ni foil that would produce a large EXAFS signal that was easy to detect as the experiment was carried out for the first time. A 25 m*M* $NiCl_2$ solution, held in a 2 mm-thick perspex container with Kapton windows, was used later to test the performance of the system under more realistic conditions. The Ni foil and the $NiCl_2$ solution were specifically chosen so that comparisons could be made (§3.1) with previous data recorded at station 9.3 using other detectors (Iles, 1998).

The absorption spectra (μ) were calculated from equation (2). In addition to the measurement of X-ray intensity incident on the detector when the sample was placed in the X-ray beam (I_t), a further three measurements were taken to make corrections to the data. The frame I_0 was taken, without the sample in place, so that variations in the X-ray flux across the detector and the amplifier gain of individual strips could be removed. Constant contributions to both the I_t and I_0 frames, such as from dark current or ADC pedestals, were removed by taking two further frames I_{tdc} and I_{0dc} without exposure to X-rays. These two frames were not identical because the I_t and I_0 frames were measured with different integration periods to ensure that the signals were of comparable size and thus gain non-linearity was minimized. A correction was not necessary for the different integration periods because for EXAFS analysis the scale is set by the size of the absorption edge. The absorption spectrum can therefore be multiplied by a constant or a constant added without hindering future analysis. To allow easy comparison with previous data sets the absorption spectra obtained with the silicon microstrip detector have been normalized so that the magnitude of the absorption edge is unity in arbitrary units. Any offset has also been removed, although in some plots showing multiple spectra a constant has been added to separate them.

$$\mu = (1/t)\ \ln\big[(I_0 - I_{0dc})/(I_t - I_{tdc})\big], \qquad (2)$$

where μ is the absorption spectrum, I_t is the X-ray intensity after attenuation by the sample, I_0 is the X-ray intensity without attenuation by the sample, I_{tdc} and I_{0dc} are the matching dark current frames for I_t and I_0, and t is related to the material thickness.

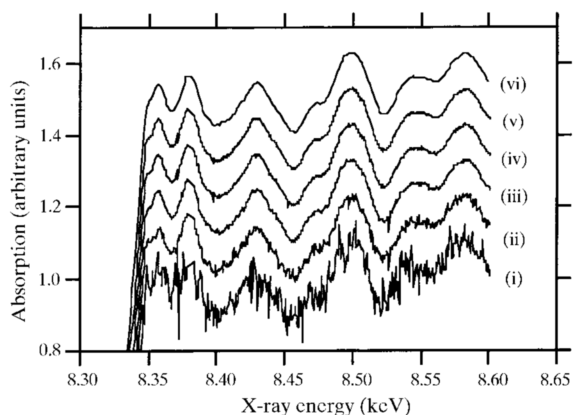

Figure 6
A plot of the absorption spectra obtained from Ni foil when Kapton film was used to attenuate the beam so that the I_t and I_0 integration periods were the same. Data were taken for (i) 1 scan, (ii) 10 scans, (iii) 100 scans, (iv) 1000 scans, (v) 10000 scans and (vi) 10000 scans with odd and even channels averaged so that these results may be compared with Fig. 5. The data sets are offset vertically by 0.1 units for clarity. Acquisition times per scan are $I_t = I_0 = 600$ μs.

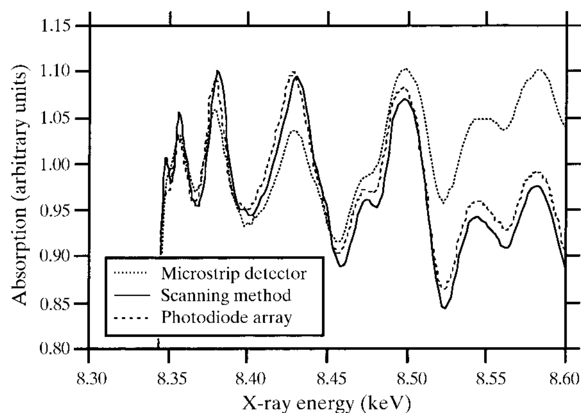

Figure 7
A comparison between the Ni foil absorption spectrum measured by the scanning method and the EDE method (photodiode array and a silicon microstrip detector). Kapton film was used to make the I_t and I_0 integration periods the same for the silicon microstrip detector, thus correcting timing errors. Acquisition times per scan for the microstrip detector are $I_t = I_0 = 600$ μs.

3.1. *Ni foil and $NiCl_2$ solution results*

A series of absorption spectra were taken for both the 5 µm Ni foil (Fig. 4) and the 25 m*M* $NiCl_2$ solution (Fig. 5). In each case the number of scans, and thus the number of integrated photons, was varied. For clarity the six spectra in each graph were separated by adding a different *y*-axis offset to each.

The series of absorption spectra for each material were taken to show the reduction in Poisson statistical noise as the number of integrated photons per frame was increased. A simple calculation of the expected Poisson noise showed that photon statistics were indeed responsible for the large noise seen on the first frame with only one scan. Increasing the number of scans per frame to ten showed an improvement, but increasing the number of scans further showed little improvement due to a systematic noise source. The last frame spectrum was composed of 10000 scans, but with the odd and even strips averaged to remove the effect of reading the odd/even strips with different MX4 chips.

The origins of the systematic noise source were timing errors between the I_t and I_0 integration periods. To remove this effect the length of the I_t and I_0 integration periods were made equal. Several layers of 125 µm-thick Kapton film were placed in the beam during the I_0 integration period so that a similar-size signal was recorded for both integration periods and thus gain non-linearity was minimized. The Ni foil absorption spectra recorded using this Kapton film method are shown in Fig. 6. There is a significant improvement over the previous measurement of the Ni foil shown in Fig. 4. Note that owing to the non-uniform attenuation by the Kapton film there is a gradual increase in the absorption cross section towards higher energy. This is shown to much greater effect in Fig. 7, which shows a comparison between the Ni foil absorption spectrum taken with a traditional scanning method and by a microstrip detector with Kapton film. A measurement made by a PDA on the same beamline is also shown for comparison. However, it should be noted that, because this was a test set-up and we wanted to maximize the flux on the detector, a source slit at the front of the beamline was not in place. Without this slit, a side pole of the 5 T wiggler can be seen which degrades the energy resolution slightly.

Non-linear gain, a further source of systematic noise, was found to depend on the layout of the 128 charge-sensitive amplifiers on the MX4 readout chip. This was due to the resistance of the tracks that connected the amplifiers at the front of the chip to the multiplexer situated at the back of the chip. The MX4 chip was designed for a different application with different priorities and hence such effects can be expected. For any future chip designed specially for EDE, special care will be necessary to ensure that systematic errors such as these are removed if they are to not dominate over statistical errors, particularly if ultimately an SNR of 10^6 is desired.

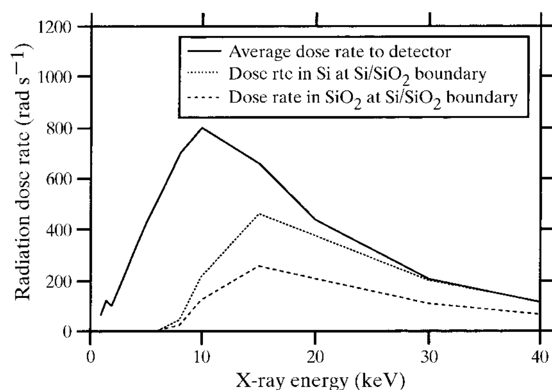

Figure 8
The average radiation dose rate received by the detector *versus* X-ray energy. Also shown is the dose rate in Si and SiO_2 at the Si/SiO_2 boundary, which is partly shielded by the silicon bulk.

3.2. *Radiation-damage results*

A specific area of concern, particularly before the beam test, was the large radiation dose that the detector would receive and the possible increase in leakage current from radiation damage. An energy transfer of ~15 eV is required to cause displacement damage to the Si crystal lattice of the substrate (Messenger & Ash, 1986). To transfer this energy from an energetic electron, created by the absorption of an X-ray, to an Si atom requires an electron of at least 165 keV. Consequently, for this application, damage was limited to the SiO_2 layer and its boundary with the silicon substrate (Fig. 2).

The effect of radiation is to increase oxide-trapped charge within the SiO_2 layer and interface states at the Si/SiO_2 boundary (Holmes-Siedle & Adams, 1993), both which contribute directly or indirectly to an increase in surface leakage current. The average dose rate in the Si substrate and the dose rate in both the Si and SiO_2 at the Si/SiO_2 boundary was calculated using the following assumptions:

(i) The detector was illuminated from the back (n-type) so that the radiation-sensitive oxide layer was partly shielded by the silicon substrate of thickness 300 µm.

(ii) The Al back of the detector was ~1 µm thick.

(iii) The length of each microstrip exposed to radiation was 1 mm.

(iv) The width of the X-rainbow matched the length of the detector (*i.e.* strip pitch × number of strips) which was 25.6 mm.

(v) The incident flux was 10^{11} photons s^{-1} over the entire detector.

The dose rate in both Si and SiO_2 at the Si/SiO_2 boundary was calculated because the oxide thickness is typically less than 1 µm, which is of comparable size to the range of energetic electrons created by photoabsorption (Fitting, 1974). The higher absorption cross section of Si relative to SiO_2 could therefore lead to a dose enhancement effect (McLean *et al.*, 1989) by energetic electrons in Si travelling into SiO_2 and generating ionization. From Fig. 8 it can be seen that below 8 keV the radiation dose to

the silicon at the Si/SiO_2 interface is relatively small (less than 40 rad s^{-1}). This is because the detector substrate has a high absorption efficiency below 8 keV and is therefore able to shield the oxide layer. Above 8 keV the detection efficiency falls rapidly. This is due to the absorption cross section, which falls in proportion to the inverse cube of the energy.

The maximum dose a detector might receive per year can be estimated on the assumption that the EXAFS equipment on the beamline is used for 50% of the year and that it is exposed to the beam for 10% of the time. This is not unreasonable given the time taken to set up equipment and to refill the storage ring. The most harmful X-ray energy for a fixed photon flux is at 15 keV because at this energy the product of absorption cross section and the X-ray energy (*i.e.* the average energy deposited per photon) is at a maximum (Fig. 8). For this X-ray energy the dose rate in SiO_2 and Si at the Si/SiO_2 boundary would be 400 and 730 Mrad year^{-1}, respectively. This is a substantial dose, but it should be noted that displacement damage is negligible and previous work (RD20 collaboration: Holmes-Siedle *et al.*, 1994) suggests that oxide charge effects saturate after ~1 Mrad, and thus possibly also interface states, so these large doses should not necessarily pose a problem. Furthermore, the device may be cooled which, although not reducing the radiation damage to the oxide layer, will lower the leakage current. Alternatively it may be periodically heated to removed trapped charge in the oxide and interface states at the Si/SiO_2 boundary by annealing.

The leakage current changed very little with irradiation and most of the changes that did occur could have been attributed to temperature fluctuations of ~1 K (Fig. 9). Data were taken over a 40 h period. The first 32 h were used to obtain the Ni foil and $NiCl_2$ solution data and to attempt to find the origin of the systematic noise. To limit radiation damage the detector was only exposed to the X-ray beam while data were collected, thus limiting exposure to the beam to just a few hours, some of which with the beam heavily attenuated. Little change was seen over this period except for an increase in dark current in the energy range 8.5–8.7 keV that occurred within the first 7 h of data collection. For the remaining part of the initial 32 h, very little change occurred.

Table 1
Approximate dose received by silicon detector during beam test.

	Dose (Mrad)	
	8.3 keV, strip 300	8.7 keV, strip 1000
Average dose received by Si bulk	3	8
Dose received by Si at the detector surface (Si/SiO_2 boundary)	0.3	1
Dose received by SiO_2 at the detector surface (Si/SiO_2 boundary)	0.2	0.6

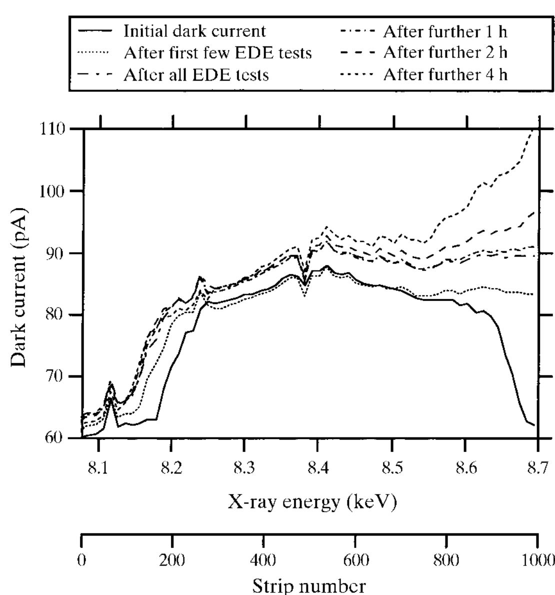

Figure 9
The change in leakage current due to irradiation.

In an attempt to observe a change in leakage current the detector was exposed to the unattenuated beam for a further period of 1 h, after which there was still little change in dark current. Further irradiation for periods of 2 and 4 h started to show a small increase in the region from 8.5 to 8.7 keV. Table 1 provides a summary of the approximate total dose received during the beam test. The maximum total dose during the beam test in Si and SiO_2 at the Si/SiO_2 boundary was between 1 Mrad and 0.6 Mrad, respectively. In theory, therefore, oxide-trapped charge should have been close to saturation, though possibly not interface states.

4. Conclusions

Absorption spectra for both an Ni foil and a 25 m*M* $NiCl_2$ solution were obtained, although further effort is required to make this a feasible alternative to the imaging systems currently used, such as the PDAs used at Daresbury Laboratory and phosphor/CCD-based imaging systems at the ESRF. It has been shown that the radiation-sensitive SiO_2/Si boundary on the surface of the silicon microstrip detector can withstand a dose of 0.6–1 Mrad without substantial increases in leakage current that would reduce the dynamic range. Furthermore, the widespread use of silicon detectors in the particle-physics community over the last two decades has allowed it to grow into a mature technology that is well understood.

At present, the electronics available for silicon detector applications are geared towards the particle-physics community whose main objective is to detect the passage of minimum ionizing particles and frequently in a synchronous environment. In contrast, EXAFS experiments require charge-integrating readout chips, with carefully controlled systematic noise sources and negligible dead

time for readout. In the future we can therefore expect effort to be required for the development of custom chips which more closely address the needs of synchrotron radiation experiments. R&D into improved readout electronics is already underway with a collaboration between CLRC, Cambridge University and Southampton University.

We thank the CLRC, PPARC and EPSRC for their financial support. We also thank John Reilly, Sarah Greenwood, Maria Khaleeq, Jeff Bizzell and Ian Clark for their technical assistance.

References

Allinson, N. M. (1989). *Nucl. Instrum. Methods*, A**275**, 587–596.
Allinson, N. M., Baker, G., Greaves, G. N. & Nicoll, J. K. (1988). *Nucl. Instrum. Methods*, A**266**, 592–597.
Bogg, D., Dent, A. J., Derbyshire, G. E., Farrow, R. C., Ramsdale, C. A. & Salvini, G. (1997). *Nucl. Instrum. Methods*, A**392**, 461–464.
Dent, A. (2000). Personal communication.
Derbyshire, G. E., Dobson, B. R., Greaves, G. N., Harris, P., Moore, P. R., Roberts, K. J., Allinson, N., Nicoll, J., Doyle, S. & Oldman, R. J. (1989). *Rev. Sci. Instrum.* **60**(7), 1897–1900.
Dobson, B. (1997). Personal communication.
Fitting, H.-J. (1974). *Phys. Status Solidi*, A**26**, 525–535.
Hagelstein, M., San Miguel, A., Fontaine, A. & Goulon, J. (1997). *J. Phys. IV (Colloque) 7*, C**2**, 303–308.
Holmes-Siedle, A. & Adams, L. (1993). *Handbook of Radiation Effects.* Oxford University Press.
Holmes-Siedle, A., Robbins, M., Watts, S., Allport, P., Brenner, R., Moser, H.-G., Roe, S., Straver, J., Weilhammer, P., Chochula, P., Mikulec, I., Moszczynski, S., Turala, M., Dabrowski, W., Grybos, P., Idzik, M., Loukas, D., Misiakos, K., Siotis, I., Zachariadou, K., Dulinski, W., Michele, J., Schaeffer, M., Turchetta, R., Booth, P., Richardson, J., Smith, N., Gill, K., Hall, G., Sachdeva, R., Sotthibandhu, S., Vite, D., Wheadon, R., Arrighi, C., Delpierre, P., Habrard, M. C., Clemens, J. C., Mouthuy, T., Avset, B. S., Evensen, L., Hanneborg, A., Hansen, T. A., Bisello, D., Giraldo, A., Paccagnella, A., Kurchaninov, L., Spiriti, E., Apsimon, R., Giubellino, P., Ramello, L., Dasilva, W. L. P., Krammer, M. & Schuster, M. (1994). *Nucl. Instrum. Methods*, A**339**, 511–523.
Iles, G. (1998). PhD thesis, ICSTM, London, UK.
Koch, A., Hagelstein, M., San Miguel, A., Fontaine, A. & Ressler, T. (1995). *Proc. SPIE*, **2416**, 85–93.
Lytle, F. W., Sayers, D. E. & Stern, E. A. (1982). *Advances in X-ray Spectroscopy*, edited by C. Bonnelle & C. Mande, pp. 267–286. Oxford: Pergamon Press.
McLean, F. B., Boesch, H. E. Jr & Oldham, T. R. (1989). *Ionizing Radiation Effects in MOS Devices and Circuits*, edited by T. P. Ma & P. V. Dressendorfer, pp. 87–192. New York: John Wiley and Sons.
Messenger, G. C. & Ash, M. S. (1986). *The Effects of Radiation on Electronic Systems.* New York: Van Nostrand Reinhold.
Sze, S. M. (1981). *Physics of Semiconductor Devices*, 2nd ed. New York: John Wiley and Sons.